2

CONF-920124--5

UCRL-JC-107442
PREPRINT

High-Power Microwave Bandwidth Broadening By Air Breakdown

David J. Mayhall
Jick H. Yee
Raymond A. Alvarez

This paper was prepared for submittal to the Ultrawideband Radar,
SPIE Laser and Radar Engineer Symposium
Los Angeles, CA
January 19-24, 1992

December 1991

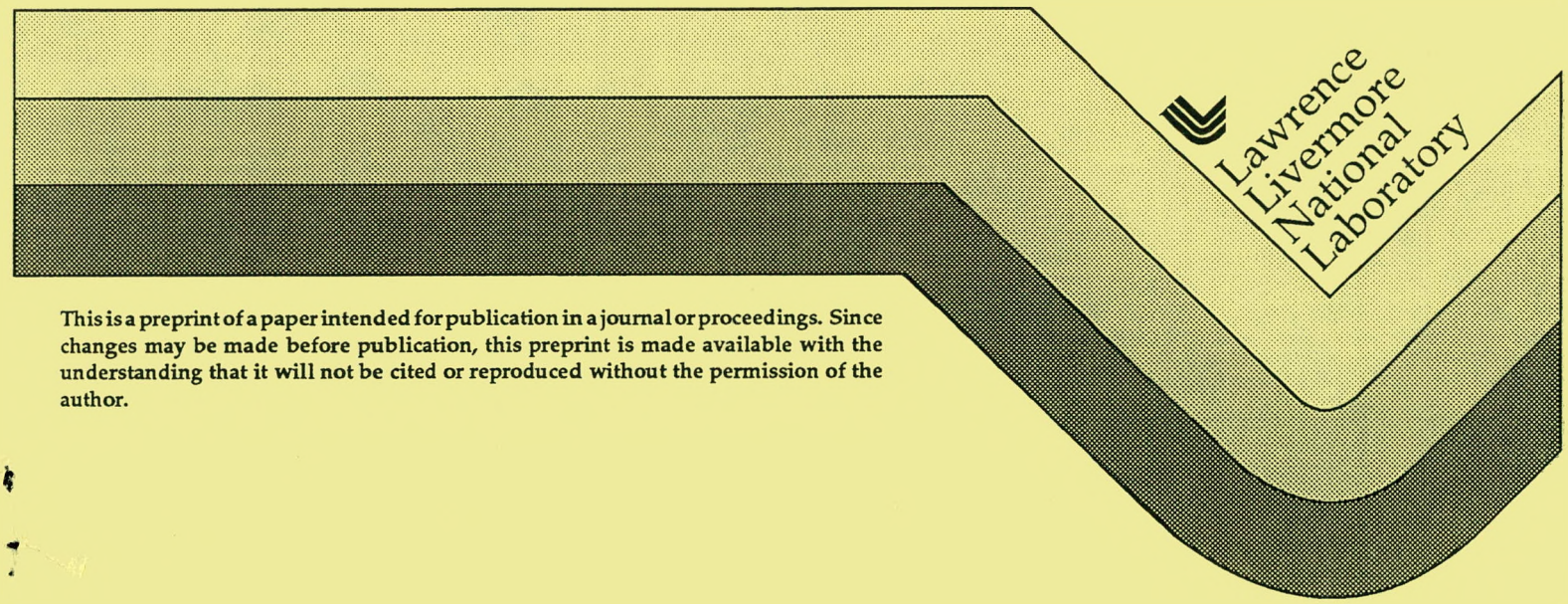

DISCLAIMER

High-power microwave bandwidth broadening by air breakdown*

UCRL-JC--107442

DE92 005246

David J. Mayhall, Jick H. Yee, and Raymond A. Alvarez

Lawrence Livermore National Laboratory
P. O. Box 808, Mail Code L-156, Livermore, CA 94551

ABSTRACT

Wideband, high-power microwave pulses are expected to have important applications in the future. One of these applications is ultra-wideband radar. The wide bandwidth should generate increased information for target characterization and identification. The high power should result in increased target detection range for conventional targets and targets with reduced signatures.

A way to generate wideband, high-power microwave pulses with relatively conventional technology is to tail erode high-power pulses by passage through a low-pressure air cell. In this process, the tails of short (3 – 10 ns), high-amplitude (>1 MV/m) pulses are removed. This erosion shortens the pulses and generates transmitted pulses with broadened bandwidths. The pressure must be matched to several incident pulse characteristics to create enough electron density to cause strong tail erosion. The important pulse characteristics are amplitude, frequency, pulse length, and pulse shape. Tail erosion of microwave pulses in the earth's atmosphere has previously been examined with one-dimensional, finite difference computer calculations.[1-3] Experiments on tail erosion in a rectangular waveguide have verified two-dimensional (2D), finite difference computer calculations.[4,5]

We have shown experimentally that tail erosion from air breakdown broadens the 3 dB bandwidths of 2.8608 GHz incident pulses in a rectangular waveguide at 3.5 torr. The incident pulse amplitude varied from 0.67 – 1.16 MV/m. The pulse bandwidth increased from 0.147 GHz by 0.0097 – 0.039 GHz or 0.34 – 1.4% relative. The incident bandwidth was 5.12% relative to the incident carrier frequency. This experimental broadening was simulated with a 2D, electromagnetic, electron fluid computer code for avalanche ionization. The simulation predicted bandwidth broadening by 0.029 – 0.13 GHz or 1.0 – 4.4% relative for a peak initial electron density of 10 electrons/cm^3. Although the measured and calculated transmitted electric field envelopes were in close agreement, the calculated bandwidths exceeded those measured by 13 – 47%. Because the detectors were not fast enough to resolve individual cycles and therefore determine the local frequency across the pulses, we presently conclude that the simulation gives better estimates of reality than do the measurements.

The computer code gives predictions of the bandwidth broadening of 3.5 ns incident pulses at 3.5 torr for a Gaussian spatial background electron distribution with a 3 cm full width at half maximum (FWHM) in the axial direction. The peak value of the electron density distribution and its transverse FWHM are variable. Incident amplitudes of 1 – 18 MV/m and peak electron densities of 10 – 10^{11} electrons/cm^3 are considered. The transmitted bandwidth varies from 0.352 – 3.21 GHz or 12.3 – 112% relative. The transmitted spectral center frequency varies from 2.87 – 4.72 GHz. The transmitted amplitude at 54.6 cm from the input to the low-pressure section varies from 0.263 – 12.7 MV/m on the waveguide center line.

1. EXPERIMENTAL BANDWIDTH BROADENING

1.1. Experimental arrangement

The experimental demonstration of bandwidth broadening from low-pressure air breakdown was conducted at the Lawrence Livermore National Laboratory 100-MeV linac. The equipment for the generation of pulses with peak powers to 100 MW and lengths of 5 – 8 ns from a pulse compression cavity is described in detail elsewhere.[4,5] Essentially, a string of two klystrons and various pulse shaping elements fed a pulse compression cavity.[6,7] When triggered with a gas breakdown tube, the cavity delivered a pulse at 2.8608 GHz to a low-pressure, WR-284 rectangular waveguide test section. The test or interaction section was backfilled with air at 3.5 torr.

A properly located ^{60}Co gamma ray source generated highly reproducible preionization of the air in the interaction section. The background electron density from the preionization ensured highly reproducible initiation of air breakdown by incident microwave

Work performed under the auspices of the U.S. Department of Energy by Lawrence Livermore National Laboratory under Contract W-7405-Eng-48.

pulses with sufficient amplitude and length. Directional couplers, located upstream and downstream from the interaction section, led to calibrated fast back diodes for measurement of the power envelopes of the incident, reflected, and transmitted pulses into and out of the interaction section. Figure 1 shows a simplified diagram of the pulse compression cavity and the interaction section. The center

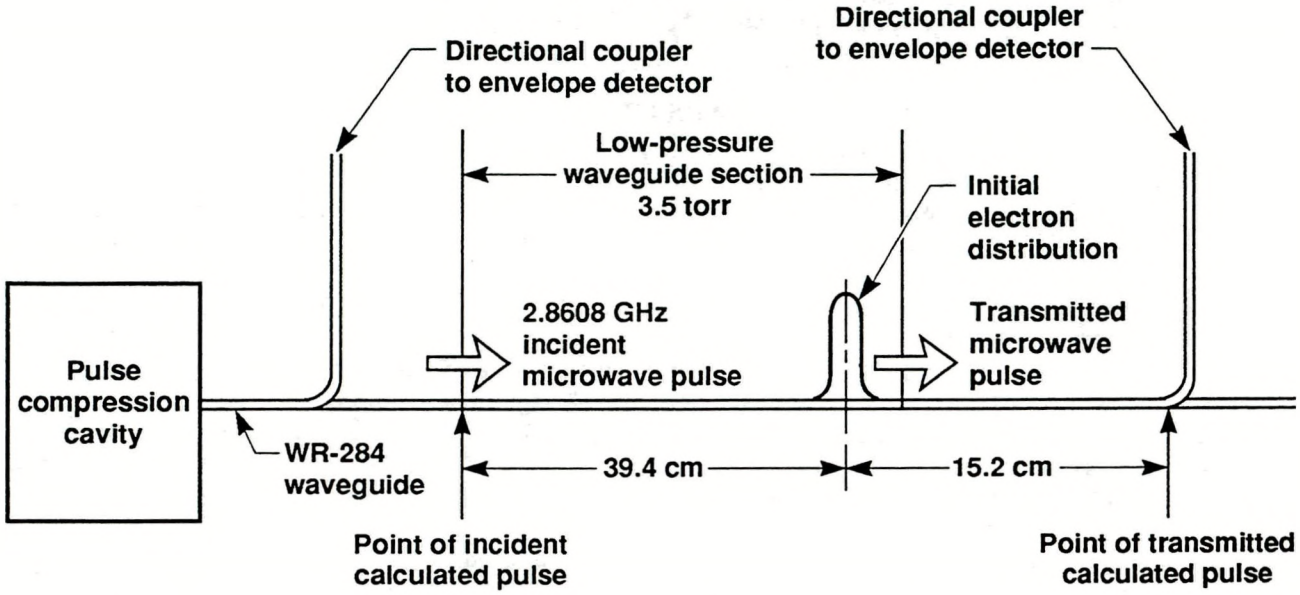

Figure 1. Simplified experimental arrangement.

of the background electron distribution was 39.4 cm from the interaction section entrance. A directional coupler sampled the transmitted pulse at 15.2 cm farther downstream.

1.2. Approximate experimental electric field waveforms

Figure 2 shows typical measured incident and transmitted electric field envelopes as dashed curves. These envelopes are for a position 0.51 cm off the waveguide center line in the waveguide "a" direction. Since the diode detectors were too slow to record each microwave cycle, they recorded the envelopes of the instantaneous average power. The electric field envelopes along the waveguide center line were extracted from the power envelopes from the known peak electric field to average power relationship for the waveguide. The electric field envelopes at 0.51 cm or one computational transverse grid spacing from the center line resulted from multiplication by $\sin(6\Delta y\pi/14\Delta y) = 0.975$, where Δy is the transverse computational grid spacing. This transverse translation was done so that measured waveforms could be compared directly with computational results.

Multiplication of the electric field envelopes by the time function $f(t) = \sin(2\pi f_c t)$ gave first order approximations to the electric field waveforms at the detectors. The quantity f_c is the incident carrier frequency, and t is the time in seconds. These approximate waveforms are shown in Fig. 2 as the solid curves. These waveforms are not the true waveforms since the cavity imparts a chirp to the output pulse.[5] In addition, waveguide dispersion causes the high-frequency spectral components to travel faster than the low-frequency components as the incident pulse travels from the cavity to the incident detector. Such dispersion causes a sufficiently short pulse to spread out temporally and undergo a decrease in amplitude in travel along the waveguide. The local frequency across a short pulse changes as the pulse traverses the waveguide. The distribution of local frequency at the detectors was unknown and could not be determined because of the lack of detector time resolution. In addition, the phase angles of the first cycles were unknown and were taken as zero.

Figure 2b shows an estimated measured transmitted electric field waveform. Air breakdown erosion has removed much of the tail of the incident pulse. Also the front of the transmitted pulse is longer than that of the incident pulse. This is likely due to waveguide dispersion. The transmitted amplitude at 1.04 MV/m is less than the incident amplitude of 1.12 MV/m. This decrease is due to a combination of dispersion and tail erosion.

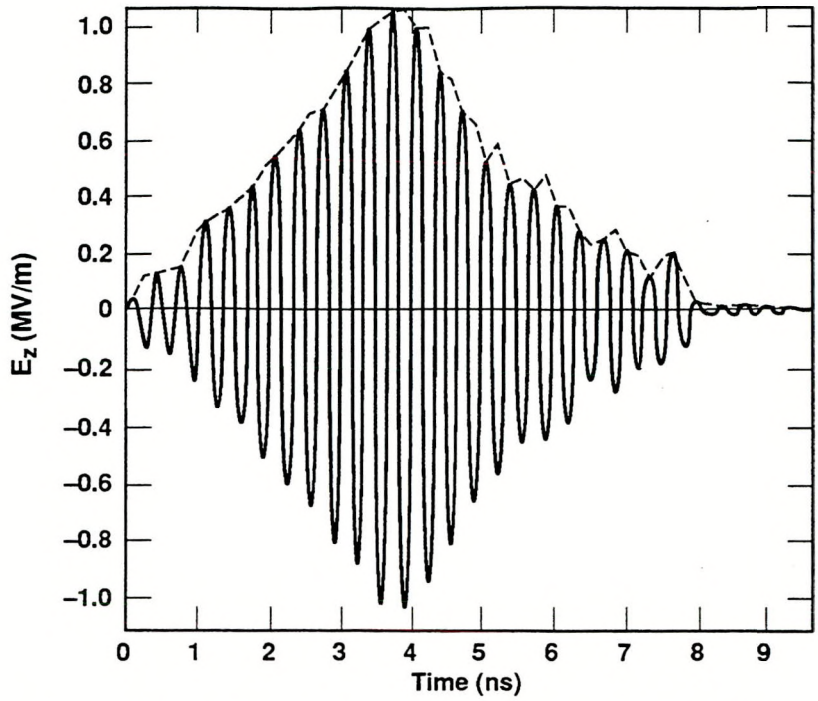

a. Measured incident envelope times sin ($2\pi \times 2.8608 \times 10^9$ t).
Max input E_z field = 1.057 MV/m; min E_z field = –1.119 MV/m.

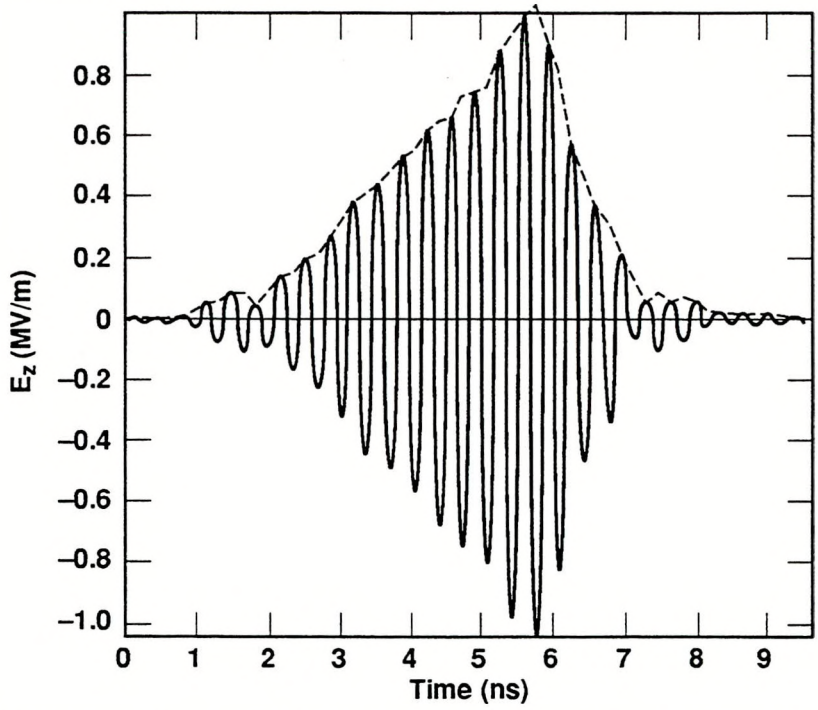

b. Measured transmitted envelope times sin ($2\pi \times 2.8608 \times 10^9$ t).
Max transmitted E_z field = 0.9984 MV/m; min E_z field = –1.043 MV/m.

Figure 2. Estimated measured pulses.
Electric field at 0.51 cm off waveguide center line.
1.164 MV/m incident amplitude on waveguide center line.
The dashed curves are the experimental envelopes.

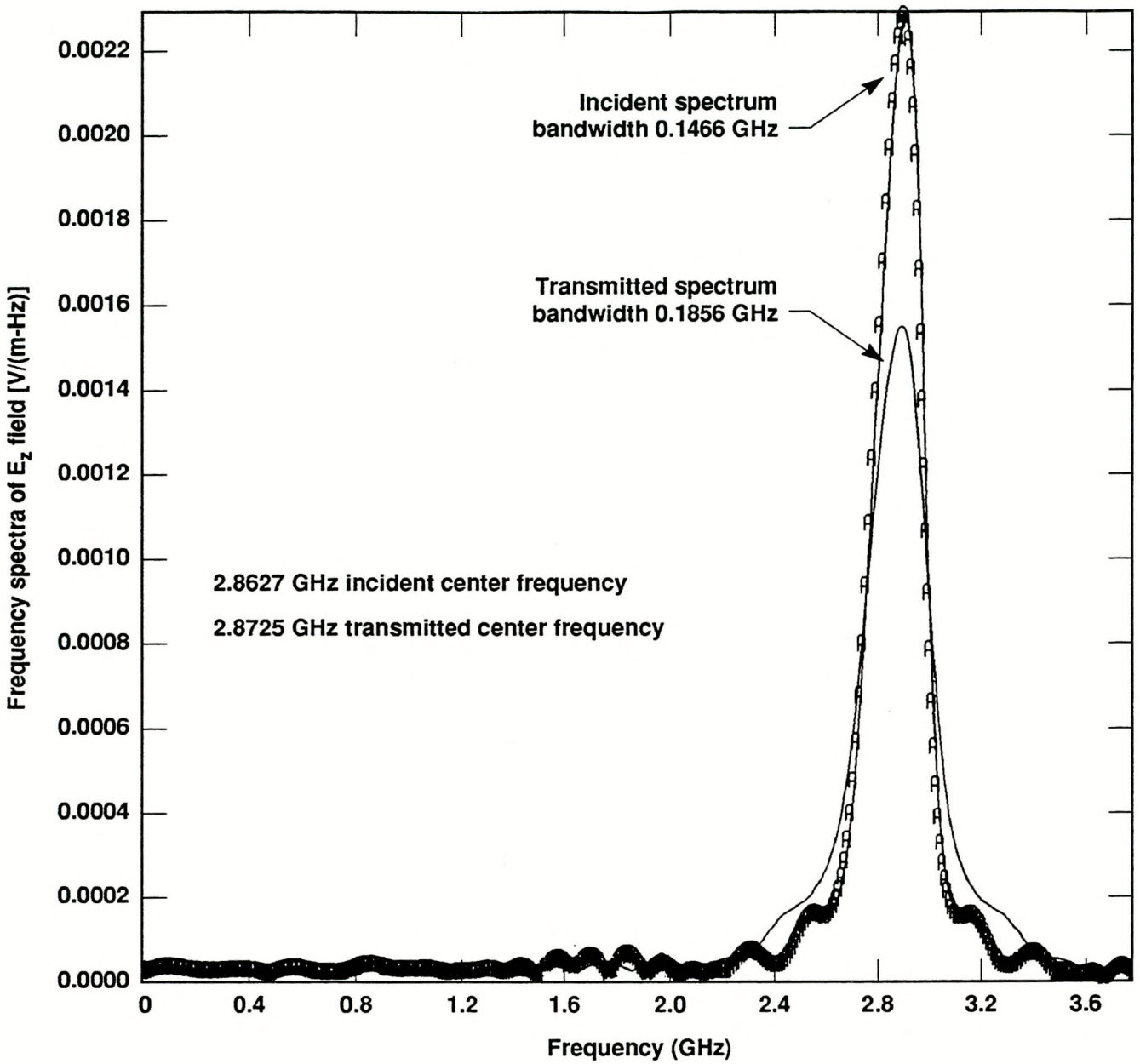

Figure 3. Estimated measured incident and transmitted frequency spectra. 1.164 MV/m incident amplitude on waveguide center line.

1.3. Experimental bandwidth broadening

Figure 3 shows the frequency spectra of the waveforms in Fig. 2. The top curve is the incident spectrum. It has a 3 dB bandwidth or a bandwidth between points at 0.707 times the spectral peak value of 0.147 GHz. This is 5.12% relative to the incident carrier frequency of 2.8608 GHz. We define the spectral center frequency of a pulse as the frequency of the spectral maximum value. The center frequency of the incident pulse is 2.863 GHz.

The lower amplitude curve in Fig. 3 is the transmitted spectrum. It has a 3 dB bandwidth of 0.186 GHz or 6.49% relative. The transmitted center frequency is 2.873 GHz. Tail erosion has caused an upward shift in the center frequency of 0.0102 GHz. Such an upward shift is expected since the tail of the pulse is cut off and high-frequency spectral components are thus injected into the back of the pulse.

Experimental results for the bandwidth broadening of three incident pulses are shown in Table 1. The incident pulses had very similar envelopes, but different amplitudes. The pulses in Fig. 2 are for 1.16 MV/m of incident amplitude. The transmitted bandwidths vary from 0.156 – 0.186 GHz (5.46 – 6.49% relative). The experimental transmitted bandwidths thus differ from the incident bandwidth of 0.147 GHz by 0.0097 – 0.039 GHz (0.34 – 1.4% relative).

Table 1. Experimental 3 dB bandwidth broadening.

Estimated measured transmitted bandwidths

Incident amplitude (MV/m)	Absolute bandwidth (GHz)	Relative bandwidth (%)
0.6679	0.1563	5.46
1.022	0.1856	6.49
1.164	0.1856	6.49

2. COMPUTATIONAL BANDWIDTH BROADENING

2.1. Computational arrangement

A 2D, finite difference, electromagnetic, electron fluid computer code for avalanche ionization in low-pressure air due to TE_{mo} modes in rectangular waveguides simulates bandwidth broadening from tail erosion. The details of this code have been previously described.[4] Three of the governing equations are the Maxwell curl equations in rectangular coordinates for H_x, H_y, and E_z with spatial derivatives in x and y. The coordinate x is along the waveguide axis, y is along the "a" or long transverse direction, and z is along the "b" or short transverse direction. The remaining three of the governing equations are for continuity, momentum, and energy conservation of the electron fluid.

Figure 2a shows a typical input pulse for simulation with the electron fluid code. A piecewise linear approximation to this pulse, weighted by the function sin ($y\pi/a$), was fed into the input side of the finite difference grid. The quantity a is the inner diameter of the waveguide in the long transverse direction. The pressure was 3.5 torr, and the low-pressure waveguide section was 54.6 cm long. A high-pressure section at 1 atm followed the low-pressure section. The high-pressure section extended to 2.54 m from the input side of the grid. An initial electron density distribution was centered at 39.4 cm from the grid input. This distribution was taken to be Gaussian in both the axial and transverse directions. The FWHM in both directions was assumed to be 3 cm. The peak initial electron density was assumed to be 10 electrons/cm^3. After encountering the assumed electron density distribution, the incident pulse initiated electron avalanching and air breakdown and experienced tail erosion. The tail-eroded transmitted pulse then travelled 15.2 cm down the waveguide, where it was sampled in time to give the transmitted pulse.

2.2. Computational bandwidth broadening

Figure 4b shows a calculated transmitted electric field waveform at 0.51 cm off the waveguide center line for the incident center line amplitude of 1.16 MV/m. Figure 4a shows the corresponding measured transmitted electric field waveform. The tail erosion is more severe for the calculated pulse. The calculated amplitude of 1.01 MV/m is 3.16% lower than the measured amplitude. This difference is most likely due to the slightly stronger tail erosion in the calculation. The measured waveform shows more dispersive spreading at the noise of the pulse and a relatively constant local frequency across the pulse in time. The calculated pulse shows a noticeably lower local frequency at the tail of the pulse, as compared to that at the front of the pulse.

Figure 5 shows the frequency spectra of the calculated incident and transmitted waveforms. The upper curve is the incident spectrum, which has a 3 dB bandwidth of 0.147 GHz. The lower curve is the calculated transmitted spectrum with a 3 dB bandwidth of 0.274 GHz or 9.56% relative to the incident carrier. This calculated bandwidth is 47.4% greater than the estimated measured bandwidth. The main reason for this difference is that the approximate analysis of the experimental average power envelope probably underestimates the transmitted bandwidth. The multiplication of the experimental envelope by the constant-frequency sine function ignores the movement of high-frequency components toward the front of the pulse during transit from the low-pressure section entrance

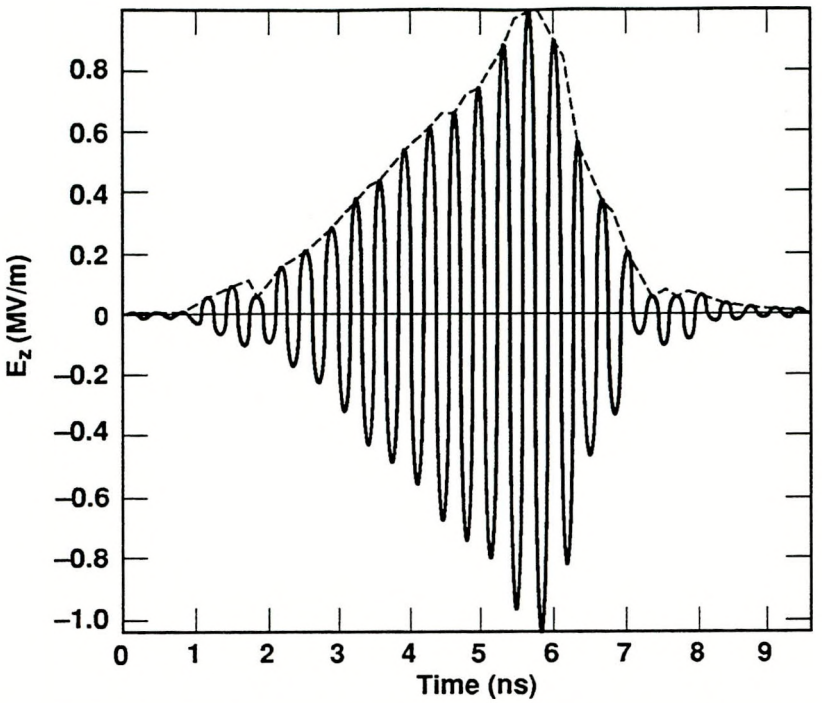

a. Measured transmitted envelope times sin ($2\pi \times 2.8608 \times 10^9$ t).
Max transmitted E_z field = 0.9984 MV/m; min E_z field = –1.043 MV/m.

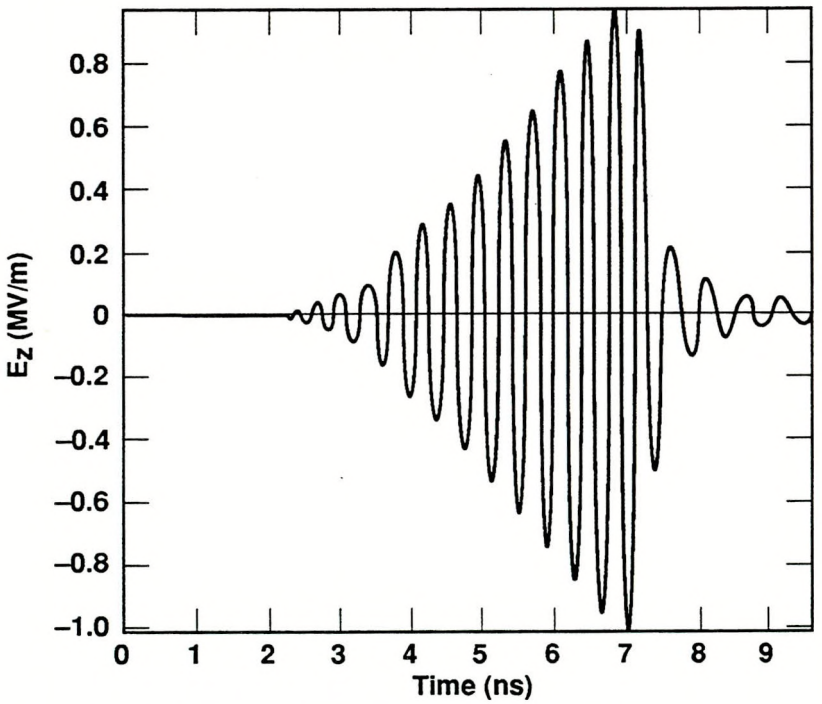

b. Calculated transmitted pulse; 54.6 cm from input.
Max transmitted E_z field = 0.9696 MV/m; min E_z field = –1.010 MV/m.

Figure 4. Transmitted pulses.
Electric field at 0.51 cm off waveguide center line.
1.164 MV/m incident amplitude on waveguide center line.
The dashed curve is the experimental envelope.

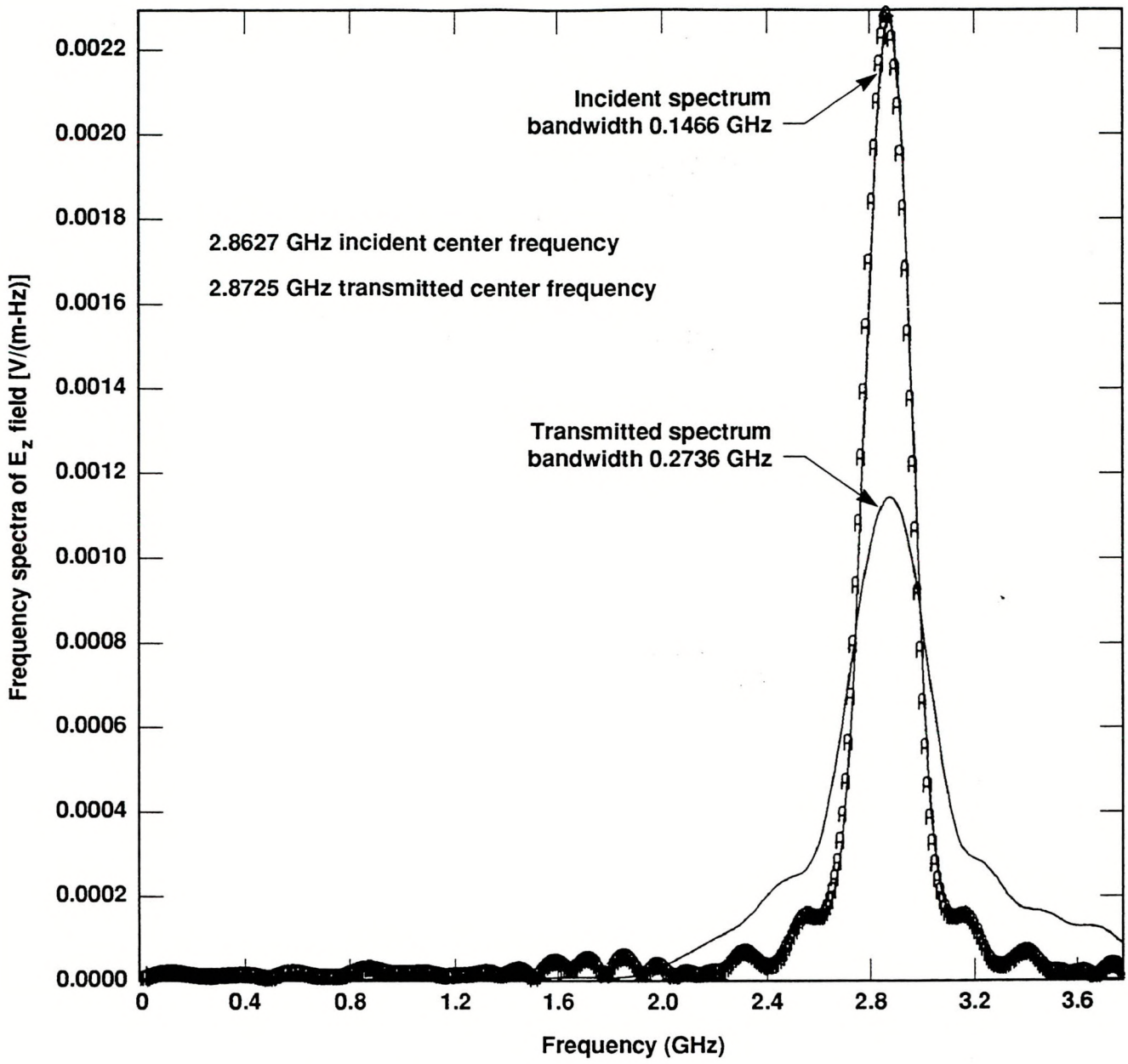

Figure 5. Calculated incident and transmitted frequency spectra. 1.164 MV/m incident amplitude on waveguide center line.

to the site of the breakdown and the injection of high-frequency components into the tail of the pulse due to the tail erosion. The movement of the injected high-frequency components forward from the tail of the pulse in transit from the breakdown site to the transmitted pulse detector is also ignored. This multiplication thus neglects the variation of the local frequency across the pulse. We believe that the computer simulation picks up both the redistribution of the local frequency due to waveguide dispersion and the injection of high-frequency spectral components from the tail erosion. Previous simulations have indicated the introduction of high frequencies at the tail of the pulse.[4] Calculated waveforms at 0.8 torr show such frequencies moving forward through the transmitted pulse and near the front of the reflected pulse. The movement of high-frequency components even causes transient enhancements of the electric field amplitude over the incident amplitude. Enhancements of up to 15% have been noted at 0.8 torr.[4]

Table 2 gives a comparison of transmitted bandwidths from the computer simulation with those from the analysis of the experimental measurements. The incident amplitude on the waveguide center line is given in the first column. The experimental

bandwidths are given in the second and third columns, and the calculated bandwidths are shown in the fourth and fifth columns. The reference for the relative bandwidths is the incident carrier frequency of 2.8608 GHz. The sixth column gives the percent difference between the calculated and measured bandwidths. This difference increases as the incident amplitude and the amount of tail erosion increase. The simulation predicts bandwidth broadening by 0.0293 – 0.127 GHz or 1.02 – 4.44% relative. Tail erosion should increase with increasing incident amplitude. This increasing tail erosion should produce increasingly shorter transmitted pulses and increasingly broader transmitted bandwidths. The increasing disagreement in transmitted bandwidth between the experiment and the simulation with increasing incident amplitude tends to corroborate the hypothesis that the lack of local frequency resolution in the measurements leads to underestimation of the broadness of the transmitted bandwidth. The code is thus believed to give better estimates of the bandwidth broadening than does the approximate analysis of the measured envelopes.

Table 2. Comparison of experimental and computational bandwidth broadening.

Transmitted bandwidths

Incident amplitude (MV/m)	Estimated measured bandwidth		Calculated bandwidth		Percent difference between calculated and measured bandwidths (%)
	Absolute (GHz)	Relative (%)	Absolute (GHz)	Relative (%)	
0.6679	0.1563	5.46	0.1759	6.15	12.5
1.022	0.1856	6.49	0.2540	8.88	36.9
1.164	0.1856	6.49	0.2736	9.56	47.4

3. PREDICTION OF BANDWIDTH BROADENING OF 3.5 NS-LONG PULSES

3.1. Computational arrangement

The equipment can generate microwave pulses with a 10 – 90% rise time of 0.4 ns. Computer simulations have been performed with incident pulses of this rise time to estimate the amount of bandwidth broadening which can be expected from the experimental equipment. The pulses from the pulse compression cavity are assumed to rise linearly in 0.5 ns and then fall linearly in 3.0 ns. The present single cavity can generate incident amplitudes up to about 10 MV/m. A second cavity in parallel with the present one could increase the peak amplitude to about 20 MV/m. Therefore, incident amplitudes up to 18 MV/m are used. The computational conditions are generally the same as those for the previous experimental simulations. The peak of the Gaussian spatial background electron density distribution varies from $10 - 10^{11}$ electrons/cm^3.

A number of types of preionization could be used for experimental generation of the assumed background electron distribution. Possible sources are gamma, X-ray, and UV radiation, as well as plasma guns and flashboards. Use of pulsed laser beams might be very convenient.[8] The deposition of the background electrons is assumed to be instantaneous on the nanosecond-time scale of the incident microwave pulse. The carrier frequency of the incident pulse is 2.8608 GHz. The 3 dB bandwidth of the incident pulse is 0.342 GHz or 12.0% relative. The incident center frequency is 2.863 GHz or 100.06% relative. Figure 6a shows an incident pulse with an amplitude of 10.0 MV/m on the waveguide center line. The amplitude in Fig. 6a is 9.45 MV/m because the pulse is calculated at 0.51 cm transversely off the waveguide center line.

3.2. Computational results

Figure 6b shows the transmitted pulse for a center line incident amplitude of 10.0 MV/m, electron distribution FWHMs of 3 cm in the axial and transverse directions, and a peak electron density of 10^9 electrons/cm^3. Strong tail erosion is evident, as is some dispersive spreading at the front of the pulse. Higher frequencies are present at the front of this pulse, while lower frequencies occur

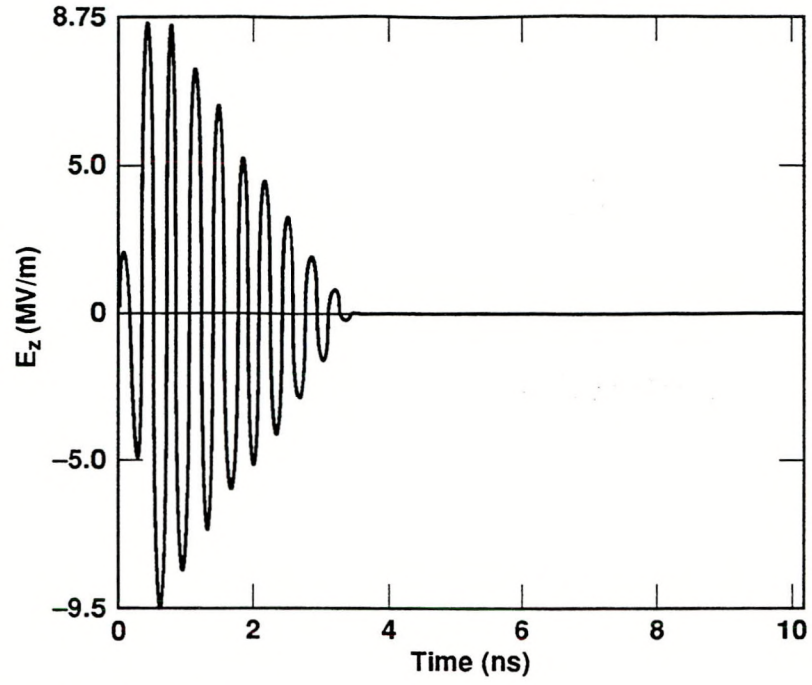

a. Incident pulse.
Max input E_z field = 8.753 MV/m; min E_z field = –9.453 MV/m.

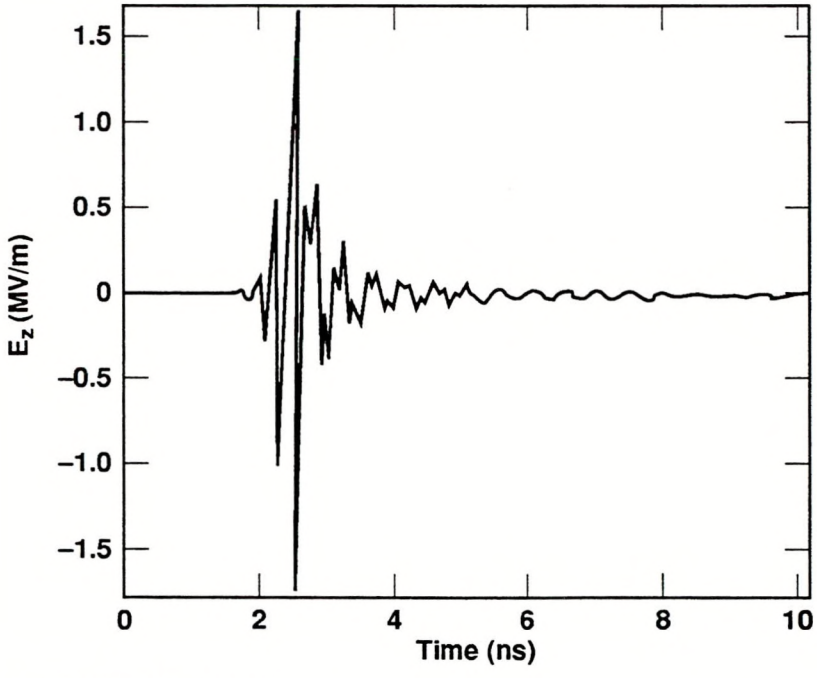

b. Transmitted pulse.
Max transmitted E_z field = 1.671 MV/m; min E_z field = –1.774 MV/m.
Pulse occurs at 54.6 cm from the input port.
Initial electron density distribution: peak value = 10^9 electrons/cm^3, axial FWHM = 3 cm, transverse FWHM = 3 cm.

Figure 6. Calculated fast rise time pulses.
Electric field at 0.51 cm off waveguide center line.
10 MV/m incident amplitude on waveguide center line.

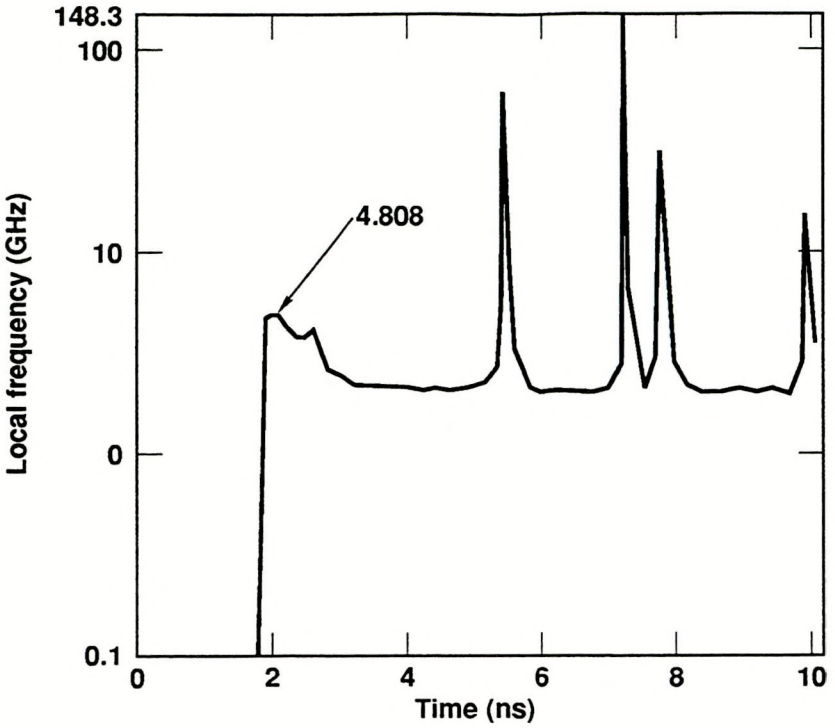

a. Distribution with high-frequency oscillations included.

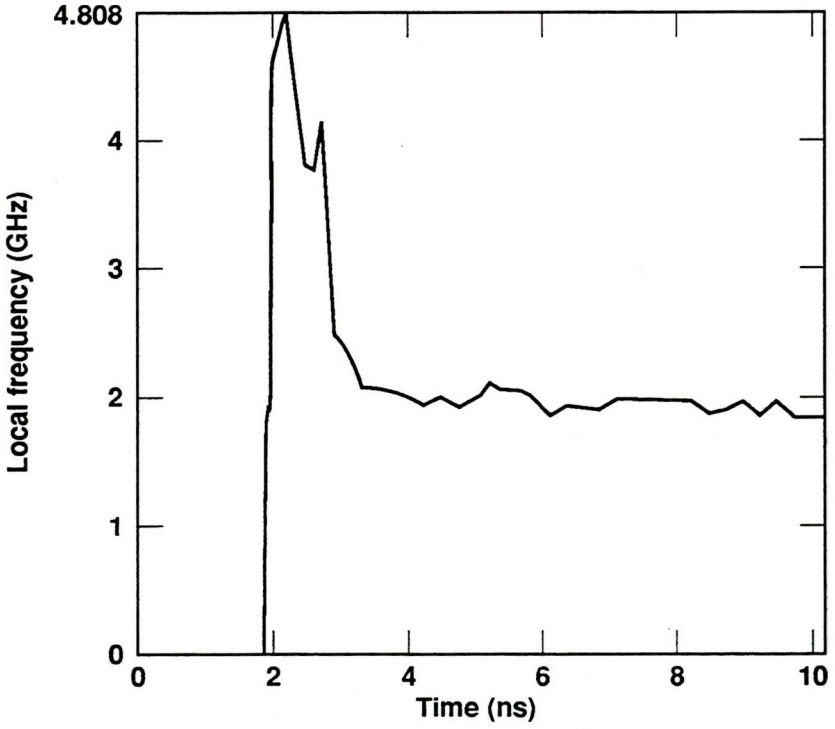

b. Distribution with high-frequency oscillations removed.

Figure 7. Local frequency distribution across the transmitted pulse.
The E_z waveform is shown in Figure 6b.
Initial electron density distribution:
peak value = 10^9 electron/cm^3, axial FWHM = 3 cm,
transverse FWHM = 3 cm.

in the tail. Low-amplitude, high-frequency oscillations also occur in the tail of this pulse. These high-frequency oscillations are not present in every transmitted pulse. They seem to occur for amplitudes greater than about 8 MV/m for the greater peak electron densities. The transmitted amplitude is 1.77 MV/m at 54.6 cm from the grid input at 0.51 cm off the waveguide center line. Correction to the center line by multiplication by 1.03 gives 1.82 MV/m for the transmitted center line amplitude.

Figure 7a shows a plot of the distribution of the local frequency across the transmitted waveform. A linear interpolation algorithm estimates the time of the zero crossings from the calculated electric field-time data pairs. The peak frequency of the low-amplitude oscillations in the pulse tail is 148 GHz. Figure 7b shows the variation of the local frequency when the high-frequency oscillations are removed. The frequency at the front of the pulse is 4.81 GHz. After about a nanosecond, the local frequency drops to around 2 GHz and then continues fall off slowly in the long, dispersed tail of the pulse.

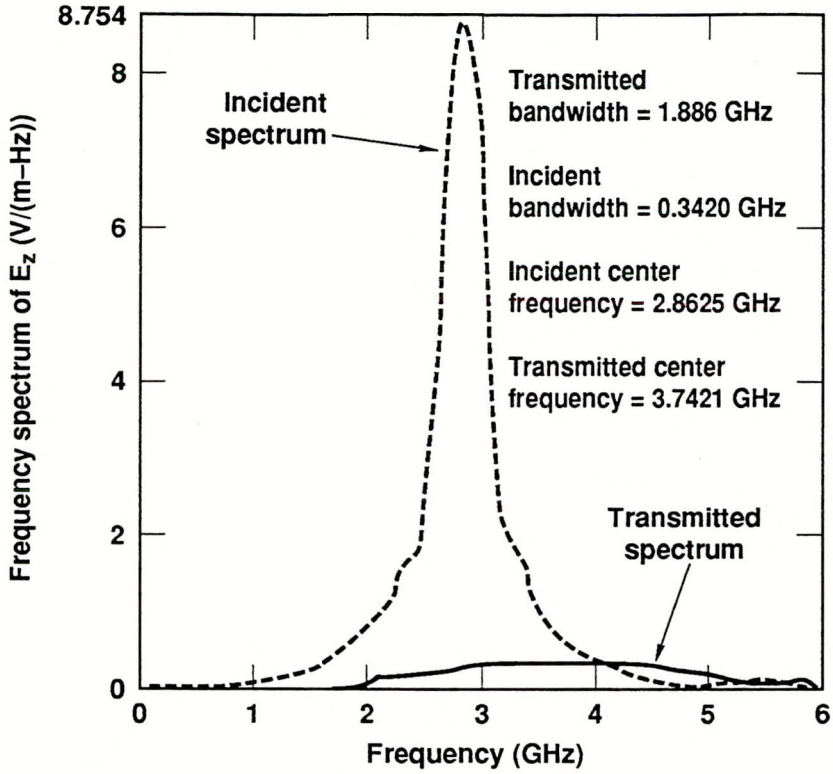

Figure 8. Frequency spectrum of the transmitted pulse. The E_z waveform is shown in Figure 6b. Initial electron density distribution: peak value = 10^9 electrons/cm^3, axial FWHM = 3 cm, transverse FWHM = 3 cm.

Figure 8 shows the incident and transmitted frequency spectra for this simulation. The incident spectrum is the upper curve. The transmitted spectrum is the much lower, much broader curve. The transmitted 3 dB bandwidth is 1.89 GHz or 65.9% relative. The transmitted center frequency is 3.74 GHz or 131% relative.

Figure 9 shows the transmitted bandwidth versus the incident center line amplitude. The parameter is the peak background electron density. The maximum transmitted bandwidth is 3.21 GHz at 11.5 MV/m incident amplitude and 10^{11} electrons/cm^3 peak electron density. The corresponding relative bandwidth is 112%, which is a very large value.

Figure 10 shows the variation of the transmitted center frequency with incident center line amplitude. The same general trends occur as for the transmitted bandwidth. The peak transmitted center frequency is 4.72 GHz or 1.65 times the incident center frequency.

Figure 11 gives the variation of the transmitted pulse amplitude on the waveguide center line 54.6 cm downstream from the input port as the incident center line amplitude increases. Figure 12 shows the variation of the transmitted pulse amplitudes at 54.6 cm and 69.8 cm downstream from the input port for 10^9 electrons/cm^3 as the incident amplitude increases. For a given incident amplitude,

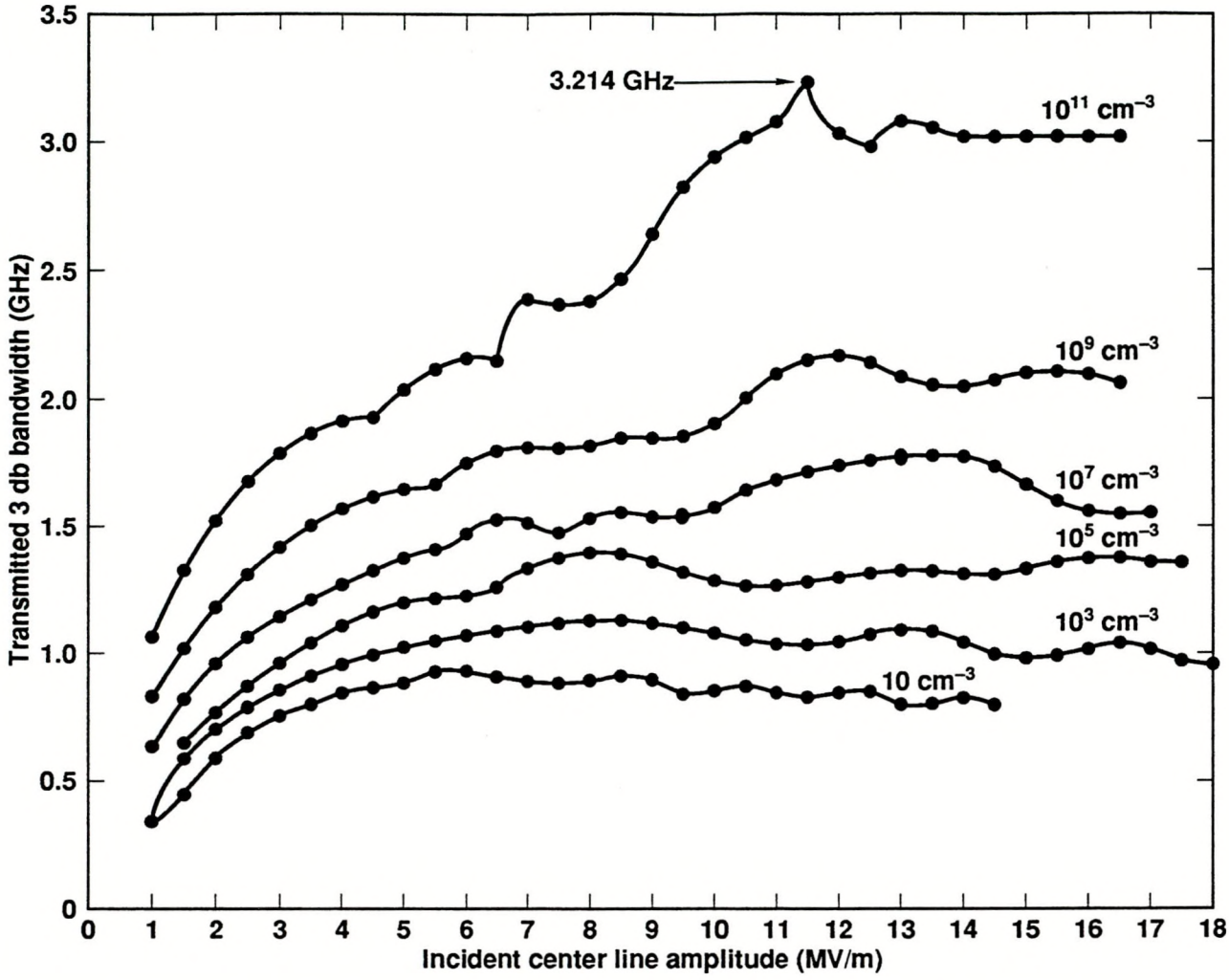

Figure 9. Transmitted 3 dB bandwidth versus incident waveguide center line amplitude. The peak initial electron density is the parameter for the curves. Initial electron density distribution: axial FWHM = 3 cm, transverse FWHM = 3 cm.

the transmitted amplitude at 69.8 cm is usually lower than that at 54.6 cm, but this is not always the case. At several points, the transmitted amplitude at 69.8 cm exceeds that at 54.6 cm. Sufficiently further downstream, presumably after all the higher-amplitude spectral components have moved to the front of the pulse due to waveguide dispersion, the amplitude of the pulse should be lower than the amplitude at 54.6 cm for all values of the incident amplitude. Beyond the air breakdown site, the system linearity of the empty waveguide should cause the transmitted bandwidth to remain constant. As the transmitted pulse travels down the waveguide, the pulse should spread out in time due to waveguide dispersion.

4. CONCLUSIONS

Approximate analysis of measured incident and transmitted air breakdown average power envelopes for pulse tail erosion at 3.5 torr in a WR-284 waveguide demonstrates bandwidth broadening, which increases with increasing incident amplitude. Electron fluid computer code simulation of the experiments in two dimensions also demonstrates bandwidth broadening. The broadening predicted by the simulation exceeds that from the experiments by up to 47%. The experimental results are believed to underestimate the real situation because the slow response of the detectors does not allow resolution of the individual microwave cycles across the pulses. Experimental resolution of the microwave cycles should yield valuable information on the distribution of local frequency in the incident and transmitted pulses.

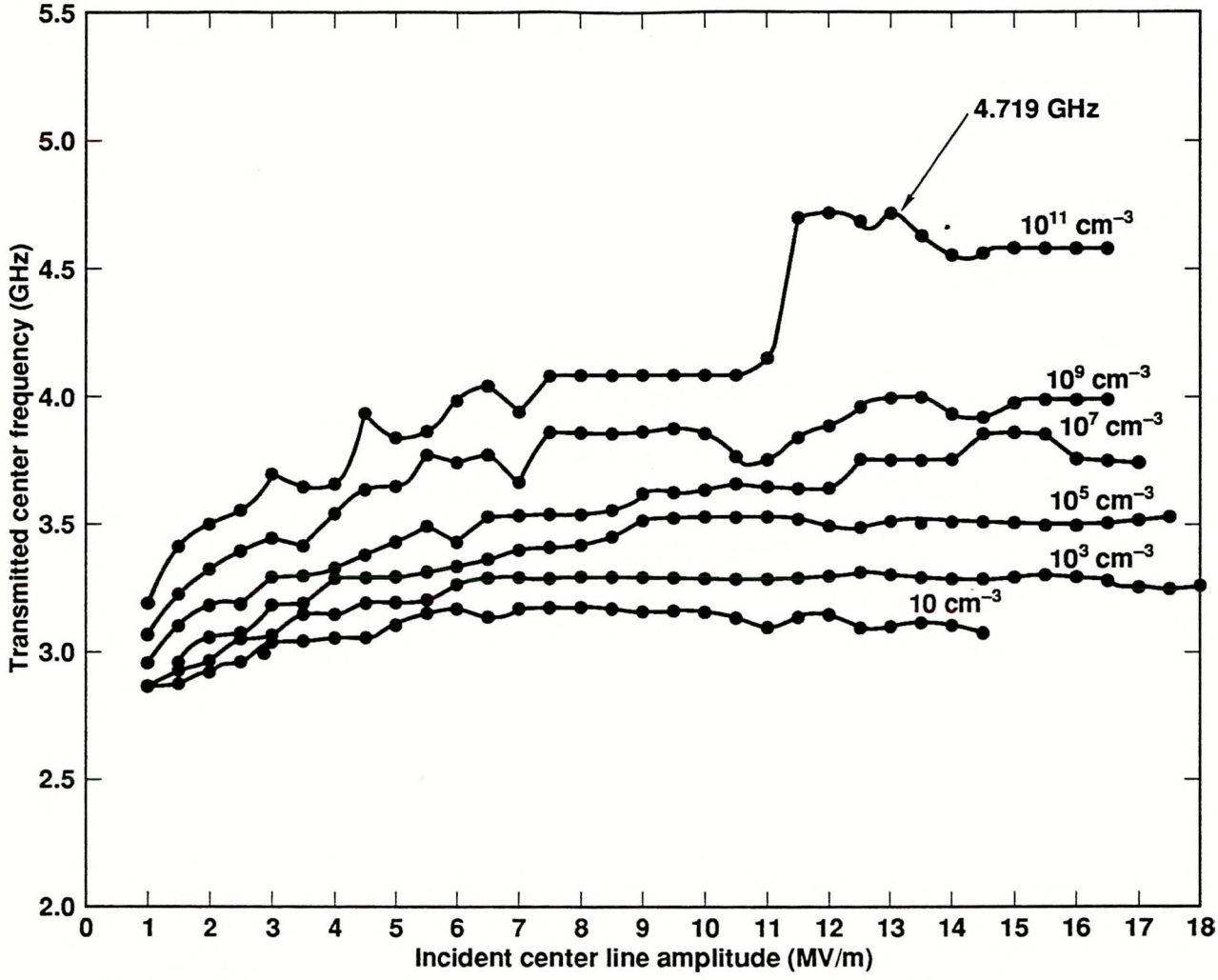

Figure 10. Transmitted center frequency versus incident waveguide center line amplitude. The peak initial electron density is the parameter for the curves. Initial electron density distribution: axial FWHM = 3 cm, transverse FWHM = 3 cm.

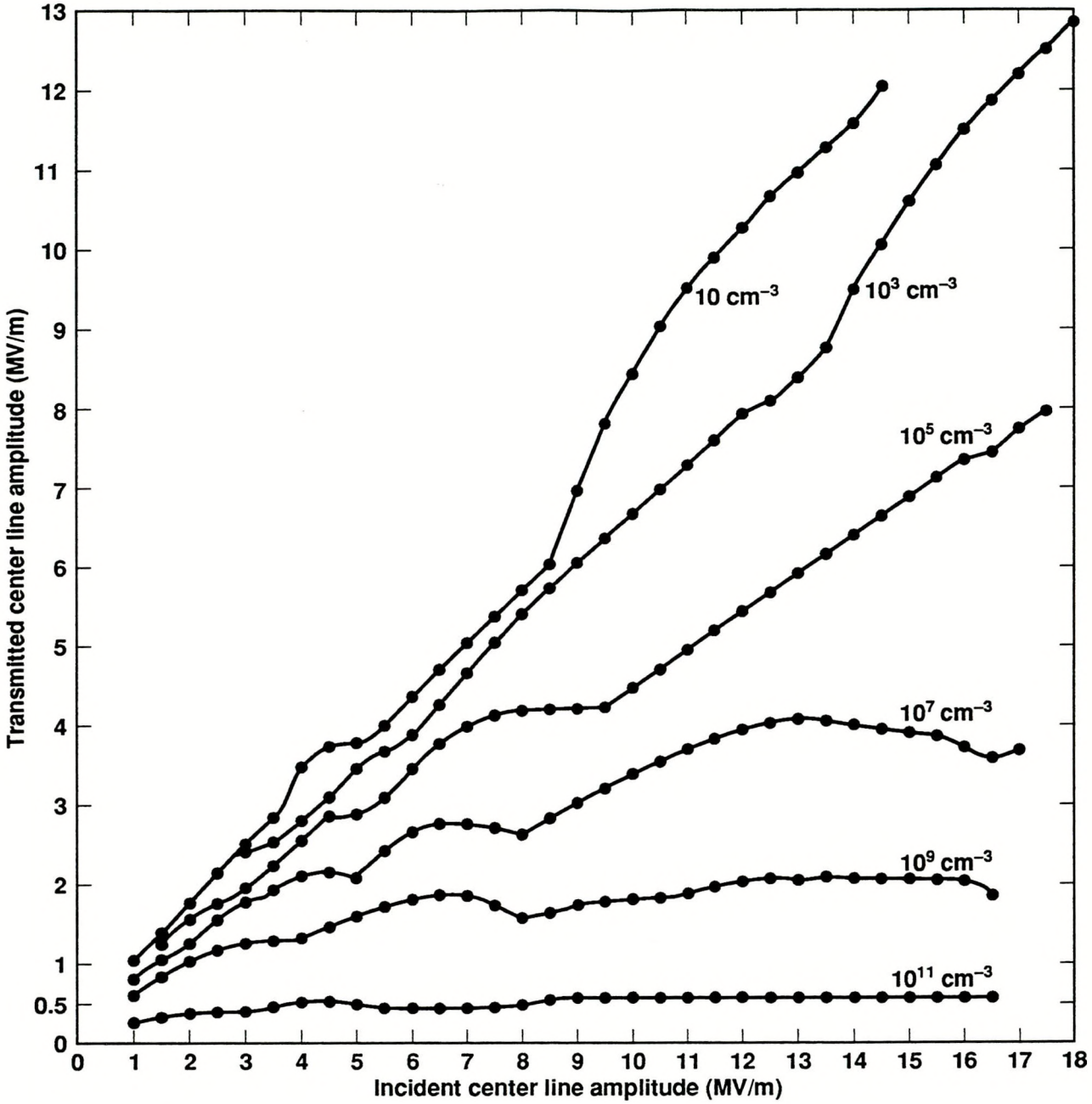

Figure 11. Transmitted center line amplitude versus incident waveguide center line amplitude at 54.6 cm from the input port.
The peak initial electron density is the parameter for the curves.
Initial electron density distribution: axial FWHM = 3 cm, transverse FWHM = 3 cm.

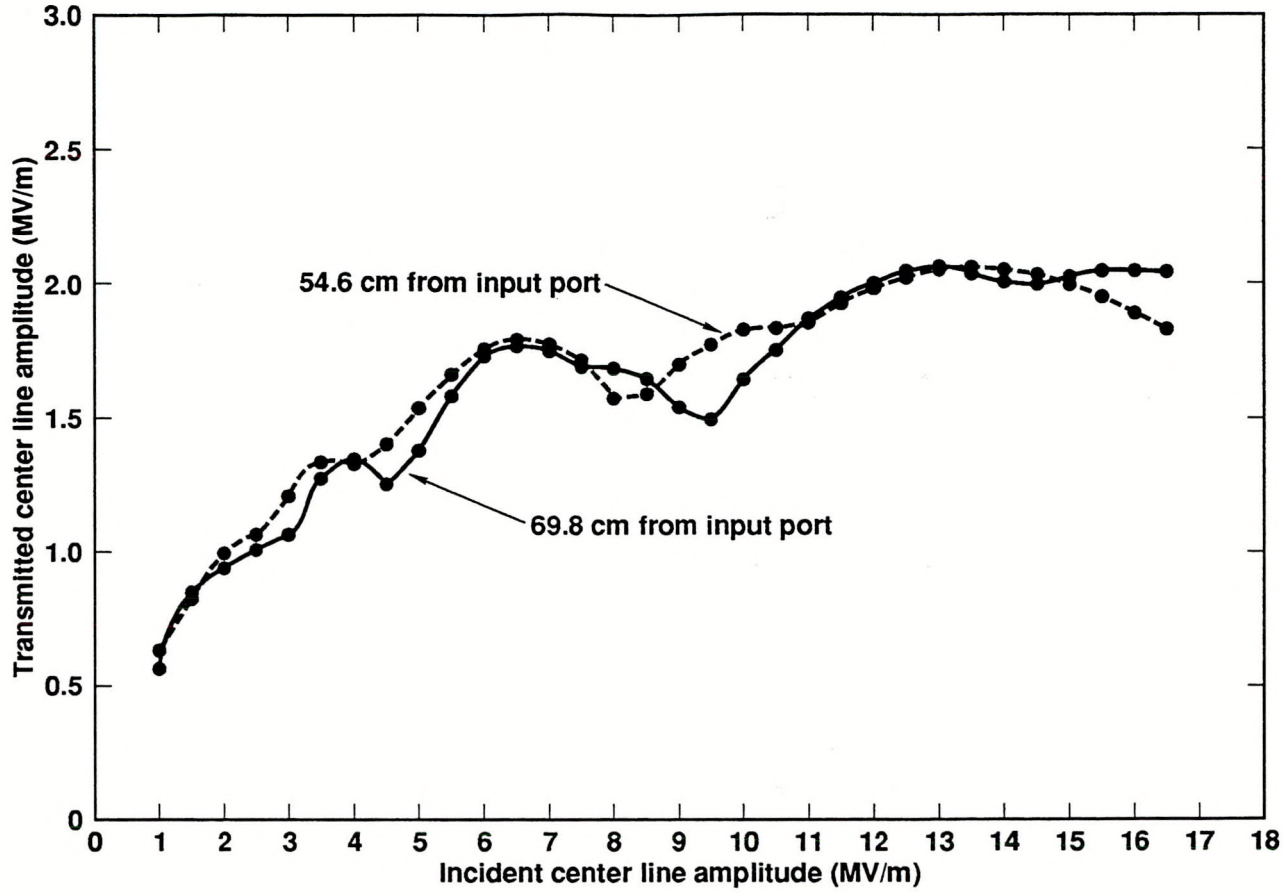

Figure 12. Transmitted center line amplitude at two axial positions versus incident waveguide center line amplitude for 10^9 electrons/cm^3 peak electron density. Initial electron density distribution: axial FWHM = 3 cm, transverse FWHM = 3 cm.

Predictions of the bandwidth broadening possible with an incident pulse shape with an 0.5 ns linear rise and a 3.0 ns linear fall are made with a series of simulations at 3.5 torr. These simulations use incident amplitudes from 1 – 18 MV/m and maximum initial electron densities from $10 - 10^{11}$ electrons/cm^3. A peak transmitted 3 dB bandwidth of 3.21 GHz or 112% relative occurs for a peak initial electron density of 10^{11} electrons/cm^3. A peak transmitted center frequency of 4.72 GHz occurs for the same peak initial electron density. Transmitted pulse amplitudes up to 12.7 MV/m occur at 54.6 cm from the input port of the low-pressure waveguide section.

Even greater transmitted bandwidths and center frequencies may occur at greater peak background electron densities and other pressures. Greater transmitted bandwidths should be possible with gases with higher ionization rates than air, such as, hydrogen, argon, and azulene. Tail erosion by air breakdown appears to be a very promising, relatively simple method for the generation of very wideband, high-power microwave pulses with relatively conventional technology. In addition, the electromagnetic, electron fluid modeling capability should allow excellent prediction of experimental results and increased insight into the physical processes which occur.

5. ACKNOWLEDGEMENTS

The authors warmly thank Dr. Paul Bolton of Lawrence Livermore National Laboratory for his experimental data on tail erosion of short, high-power microwave pulses in low-pressure air.

6. REFERENCES

1. J. H. Yee, R. A. Alvarez, D. J. Mayhall, D. P. Byrne, and J. DeGroot, "Theory of Intense Electromagnetic Pulse Propagation through the Atmosphere," *Phys. Fluids*, vol. 29, no. 4, pp. 1238–1244, April 1986.

2. J. H. Yee, R. A. Alvarez, and D. J. Mayhall, Laser Interaction and Related Plasma Phenomena, vol. 7, pp. 901–913, Plenum Press, New York, 1986.

3. G. E. Sieger, D. J. Mayhall, and J. H. Yee, Laser Interaction and Related Plasma Phenomena, vol. 8, pp. 139–148, Plenum Press, New York, 1988.

4. D. J. Mayhall, J. H. Yee, R. A. Alvarez, and D. P. Byrne, Laser Interaction and Related Plasma Phenomena, vol. 8, pp. 121–137, Plenum Press, New York, 1988.

5. D. P. Byrne, "Intense Microwave Pulse Propagation through Gas Breakdown Plasmas in a Waveguide," Ph.D. Thesis, UCRL-53764, Lawrence Livermore National Laboratory, Livermore, CA, 94551, Oct. 1986.

6. R. A. Alvarez, D. L. Birx, D. P. Byrne, E. J. Lauer, and D. J. Scalapino, "Application of Microwave Energy Compression to Particle Accelerators," *Particle Accel.*, vol. 11, pp. 125–130, 1981.

7. R. A. Alvarez, D. P. Byrne, and R. M. Johnson, "Prepulse Suppression in Microwave Pulse-Compression Cavities," Rev. Sci. *Instr.*, vol. 57, no. 10, pp. 2475–2480, Oct. 1986.

8. P. R. Bolton, R. A. Alvarez, and D. N. Fittinghoff, "Further Development of the Double Cavity Microwave Pulse Compression Source and Laser-Induced Plasma Switching," *1990 IEEE International Conference on Plasma Science*, Oakland, CA, Conference Record-Abstracts, p. 153, May 21–23, 1990.

Technical Information Department · Lawrence Livermore National Laboratory
University of California · Livermore, California 94551